A New Iodiplumbate-based Hybird Constructed from Asymmetric Viologen and Polyiodides: Structure, Properties and Photocatalytic Activity for the Degradation of Organic Dye

WANG Dao-Hua(王道华);LIN Xiao-Yan(林小燕);WANG Yu-Kang(王雨康);ZHANG Wen-Ting(张文婷);SONG Kai-Yue(宋凯悦);LIN Heng(林恒);LI Hao-Hong (李浩宏);CHEN Zhi-Rong (陈之荣)

College of Chemistry, Fuzhou University, Fuzhou 350116, *China*

ABSTRACT A new iodiplumbate/organic hybrid constructed from asymmetric viologen and polyiodides, $(PBPY\text{-}H_2)_2[PbI_4(I_3)_2]$ (**1**, PBPY = N-(propionate)-4,4′-bipyridinium), has been synthesized via solvothermal reaction and structurally determined by X-ray diffraction method. Compound **1** crystallizes in monoclinic system, space group $P2_1/c$ with M_r = 1936.72, a = 11.622(2), b = 14.839(3), c = 13.372(2) Å, β = 109.447(3)°, V = 2174.6(7) Å^3, Z = 2, D_c = 2.958 g/cm^3, F(000) = 1712, μ(Mo$K\alpha$) = 11.011 mm^{-1}, the final R = 0.0389 and wR = 0.0854 for 3866 observed reflections with $I > 2\sigma(I)$. $[PbI_4(I_3)_2]^{4-}$ mononuclear cluster of **1** features a seldom example of coordinated I_3^- donors for the lead center. Intermolecular hydrogen bonds between $[PbI_4(I_3)_2]^{4-}$ clusters and $(PBPY\text{-}H)_2^{4+}$ dimmers contribute to the formation of a 2-D layer. Its absorption spectrum was investigated, and lower energy band gap of 1.42 eV was explained by DFT calculation. Interestingly, **1** exhibits photocatalytic activity for the degradation of rhodamine B.

Keywords: organic-inorganic hybrid; iodiplumbate; asymmetric viologen; photocatalytic degradation;
DOI: 10.14102/j.cnki.0254-5861.2011-1749

1 INTRODUCTION

In the last decade, great attention has been paid to the design and synthesis of the main group metals, for example, Ge(II), Sn(II), Pb(II), Sb(III) and Bi(III), and the halide-based hybrid materials, owing not only to their versatile structure types but also to their potential applications in different fields, such as semiconductivity[1, 2], luminescence[3, 4], photo/thermochroism[5-8], and specially the emerging visible-light sensitizers for photovoltaic cells[9, 10]. The main group metal centers exhibit electronic configurations of

$d^{10}ns^2np^{2\ or\ 3}$, so they present stereochemical activities with or without the presence of ns^2 lone pair in their coordination spheres, from which many interesting properties can stem[11, 12]. Up to now, as for the anion structures of iodiplumbate, versatile structural dimensions have been observed ranging from isolated anions, infinite chains, layered perovskites to three-dimensional polymeric networks constructed from face-, edge-, or vertex-sharing PbI_6 octahedra[13]. Among mononuclear cases, only PbI_6^{4-} and PbI_4^{2-} have been reported[14, 15]. More recently, viologens (*N*,*N*′-disubstituted 4,4′-bipyridinium) have become hot materials due to their excellent electron-accepting nature, and they have been incorporated into haloplumbate system to realize photo/thermochroism functions[5-8]. Although symmetrical viologens have been widely studied in the previous work, the asymmetric viologens and their corresponding metal-halide hybrids have been rare explored[16]. N-(propionate)-4,4′-bipyridinium is a neutral inner salt with an electron-donating carboxylate group and an electron-accepting 4,4′-bipyridinium group. In this work, we introduced asymmetric viologens and polyiodides into the haloplumbate system to generate a new hybrid, $(PBPY\text{-}H_2)_2[PbI_4(I_3)_2]$, whose adsorption, band gap and photocatalytic activity were discussed.

2 EXPERIMENTAL

2. 1 Materials and methods

All of the reactants were of reagent grade and used as purchased. PBPY was self-synthesized. Elemental analyses for C, H and N were performed on a Vario MICRO elemental analyzer. IR spectra were recorded on a Perkin-Elmer Spectrum-2000 FTIR spectrophotometer (4000～400 cm^{-1}). UV-Vis spectrum was measured on a Perkin-Elmer lambda 900 UV/Vis spectrophotometer equipped with an integrating sphere at 293 K, and $BaSO_4$ plates were used as reference.

2. 2 Synthesis of PBPY

PBPY was synthesized according to a similar synthetic procedure reported[17], using 4,4′-bipyridine and bromopropionic as starting materials in the CH_3CN solvent:

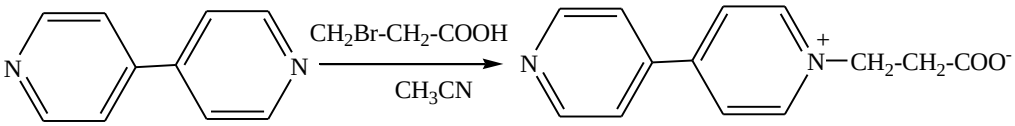

2. 3 Synthesis of $(PBPY\text{-}H_2)_2[PbI_4(I_3)_2]$ (1)

PBPY (0.2280 g, 1 mmol) and PbI_2 (0.2305 g, 0.5 mmol) were dissolved in 10 mL HI (55%) and stirred

for 30 minutes. The resultant solution was transferred and sealed in a 25 mL Teflon-lined stainless-steel reactor, which was heated at a rate of 5 ℃/h to 120 ℃ under autogenous pressure. After being maintained for 3 days, the reaction vessel was cooled to room temperature at a rate of 4 ℃/h. Black block crystals with the yield of 45.2% (0.437 g, based on Pb) were obtained and washed by ether. Anal. Calcd. for $C_{26}H_{28}I_{10}N_4O_4Pb$ (1936.72): C, 16.12; H, 1.45; N 2.89%. Found: C, 16.59; H, 1.58; N, 2.68%. IR (KBr, cm^{-1}): 3391(s), 3047(s), 2922(s), 1708(m), 1610(s), 1580(s), 1458(m), 1390(s), 1120(m), 796(s), 765(m), 550(w). Due to the higher I^- concentration in HI solution, I_3^- anions can be observed in the product.

2. 4 Computational details

The band structure calculation was based on density function theory (DFT)[18], in which wave functions were explained in a plane wave basis set, and the spin polarized version of the PW-91 GGA was employed for the exchange-correlation functional in the CASTEP code[19]. The number of plane waves included in the basis was determined by a cutoff energy E_c of 550 eV. The pseudoatomic calculations of Pb ($5d^{10}6s^26p^2$), I ($5s^25p^5$), O ($2s^22p^4$) and N ($2s^22p$) were conducted.

2. 5 Photocatalytic testing

In the degradation experiment, a 300 W Xe arc lamp equipped with a $\lambda \geqslant 420$ nm cutoff filter and an IR filter was set as the visible light source, whose output light intensity was measured as 110 mw/cm^2. During the photo-degradation experiment of RhB, 40 mg catalyst powder was suspended in 80 mL RhB solutions (concentration: 10 ppm). In order to achieve adsorption-desorption equilibrium of the organic contaminants on the catalyst surfaces before irradiation, the suspensions were magnetically stirred in the dark for 2 h until no change occurred in the UV/Vis absorption of the RhB solution. The photocatalytic performance of the catalysts was estimated by monitoring the visible absorbance (λ = 555 nm) characteristic of the target (RhB) by UV/Vis spectroscopy. The sample solutions (3 mL) were taken out at given time intervals and separated through sample filtration. The residual pollutant concentrations were analyzed by the maximum absorption band in the UV-Vis spectra of the organics. The percentage of degradation was reported as C/C_0. Here, C was the absorption of RhB at each irradiated time interval with the main peak at 553 nm, and C_0 was the absorption of the starting solution when the adsorption-desorption equilibrium was achieved.

2. 6 X-ray crystallography

Red block crystal of **1** with dimensions of 0.35mm × 0.30mm × 0.25mm was mounted on a glass fiber. The intensity data were collected on a Bruker APEX II diffractometer using a graphite-monochromated Mo$K\alpha$ radiation (λ = 0.71073 Å) at 293(2) K by an ω-2θ scan mode. In the range of $2.44 \leqslant \theta \leqslant 31.05$ °, out of the 9936

total reflections, 5548 were independent with R_{int} = 0.0258, of which 3866 were considered to be observed ($I > 2\sigma(I)$) and used in the succeeding refinement. The multi-scan absorption correction was applied. Its structure was solved by direct methods in SHELXS-97 program and refined on F^2 by full-matrix least-squares techniques using the SHELXL-97 program[20]. Hydrogen atoms of C–H were generated geometrically. The final R = 0.0389 and wR = 0.0854 ($w = 1/[\sigma^2(F_o^2) + (0.0426P)^2 + 2.0266P]$, where $P = (F_0^2 + 2F_c^2)/3$), S = 1.014, $(\Delta/\sigma)_{max}$ = 0.000, $(\Delta\rho)_{max}$ = 1.466 and $(\Delta\rho)_{min}$ = –1.264 e/Å^3. Important bond lengths are listed in Table 1, and hydrogen bond details are given in Table 2.

3 RESULTS AND DISCUSSION

3. 1 Structure description

The organic-inorganic hybrid structure of **1** is composed by $[PbI_4(I_3)_2]^{4-}$ mono-nuclear cluster and protonized $(PBPY\text{-}H)^{2+}$ cation, and intermolecular hydrogen bonds between them contribute to the formation of a 2-D layer. In the $[PbI_4(I_3)_2]^{4-}$ mononuclear cluster, the lead center adopts normal octahedral geometry coordinated by four iodine ions and two I_3^- anions. In this slightly distorted PbI_6 octahedron, four iodine ions locate at equator plane and two iodine atoms from I_3^- occupy the axial positions (Fig. 1a). The Pb–$I_{equator\ plane}$ distances range among 3.1246(6)～3.1732(6) Å, and the Pb–I_{axial} distance is 3.3177(10) Å. The I–Pb–I angles (89.836(17)～90.164(17) and 180.000(11) °) deviate slightly from ideal octahedral values of 90 ° and 180 ° (Table 1). Judging from the Pb–I distances, we can conclude that the lead center is stereochemically inactive according to Brown's model[21]. The I_3^- anion is slightly bent with the I(5)–I(4)–I(3) angle of 176.43(3) °, and the I–I distances of 2.9618(10)/2.8811(10) Å indicate a slightly asymmetrical triiodide. The cases of I_3^- anion coordination to metal centers have been observed in Cu, Pt, Ir, Ni and Hg systems[22, 23], but its coordination to Pb center is very seldom[24]. Because the synthesis environment is in strong acid, carboxyl and N atom on PBPY are protonized. The C–C, C–N and C–O bonds in $(PBPY–H)^{2+}$ cation are normal. Two pyridine rings are generally coplanar with the dihedral angle of 11.87 °. Intermolecular hydrogen bonds between two carboxyl groups of $(PBPY–H)^{2+}$ cations with the O ··O distance of 2.662(8) Å can be observed (Fig. 1b, Table 2). Based on the inter-molecular hydrogen bonds, a $(PBPY–H)_2^{4+}$ dimmer is given (Fig. 1b). N–H ··I$_{equator\ plane}$ hydrogen bonds between $[PbI_4(I_3)_2]^{4-}$ cluster and $(PBPY–H)_2^{4+}$ dimmer contribute to the formation of a 1–D chain along the *b* axis, which is further linked into a 2-D plane along the *bc* plane via C–H ··I$_{equator\ plane}$ hydrogen bonds (Table 2, Fig. 2).

3. 2 Adsorption spectrum, linear absorption optical property and band structure

In order to find the photo-response regions, the solid state diffuse-reflectance UV/Vis measurement on the as-synthesized compound was conducted, as shown in Fig. 3a. Compound **1** exhibits broad adsorption ranging from 250 to 800 nm, suggesting its adsorption in visible region and its application in visible-light catalysis. The broad range of absorption in the visible (400～600 nm) and near-infrared (600～800 nm) of **1** is special, and no such band is observed for MVI_2[25]. The presence of visible and near-infrared adsorption is assigned to the absorption of charge transfer (CT) or partial electron transfer between the $[PbI_4(I_3)_2]^{4-}$ anion and $(PBPY\text{-}H)^{2+}$ cation. In all, the intense CT bands of **1** stem from the cation and anion interactions and short contacts, for example, hydrogen bonding. The absorption peaks at 320 and 366 nm can be observed. Compared with the UV-Vis absorption spectra of bipyridine, bulk PbI_2 and relative compounds, the peak at 320 nm can be assigned to the π-π* and n-π transfer of pyridine, and the peak at 366 nm stems from PbI_6 octahedra center[26, 27].

The optical gap of **1** was assessed from its optical diffuse reflectance data, and the Kubelka-Munk functions converted from the diffuse reflectance data are plotted in Fig. 3b[28, 29]. As shown in Fig. 3b, E_g of 1.41 eV illustrates its narrow gap. Compared with that of bulk PbI_2 (2.47～2.49 eV) [30], the gap of **1** becomes narrow clearly, which might be led by the introduction of conjugated organic cations and the presence of versatile weak interactions. The lower band gap of **1** can be explained by theoretical calculation. Band structure calculation and DOS of **1** are shown in Fig. 4. The calculated band-gap value is 0.95 eV, which is generally consistent with the experimental value of 1.41 eV, taking into account the underestimation gap using generalized-gradient approximation in Kohn-Sham DFT function[31]. The DOS diagram indicates that the tops of the valence bands are mostly formed by π bonding orbital of $(PBPY\text{-}H)^{2+}$, while the bottoms of the conduction bands are almost contributed from I-5p states of I_3^- anion (Fig. 4b). This situation is different from that of viologen/metal halide system, whose CB are generally p-π* antibonding orbitals of the viologens. In other words, the introduction of I_3^- anion will result in lower band gap, which is beneficial for its photocatalytic activity.

3. 3 Photocatalytic degradation of organic pollutant

Here, N-containing dye, rhodamine B (RhB), was selected as a model pollutant for degradation experiment. The wavelength and absorption intensity changes of RhB under the irradiation of xenon-lamp with the presence of catalysts are revealed in Fig. 5a. As illustrated by Fig. 5a, with the presence of catalysts, the adsorption spectra of RhB decrease to different extents with lengthening the irradiation time, suggesting that

the degeneration reactions on RhB have occurred. Importantly, the characteristic adsorption of RhB (555 nm) shifted to 497 nm, which suggested that the degradations of dye proceeded in the presence of catalyst[32]. The peaks at 555 nm exhibited slight shift, suggesting that only deethylation of RhB has happened. Fig. 5b shows the rate of RhB degradation (measured as RhB concentration versus irradiation time) in an aqueous solution in the presence of **1**. After irradiation for 180 min, the degradation ratio is about 82.4%.

4 CONCLUSION

In summary, a new iodiplumbate/organic hybrid constructed from asymmetric viologen and polyiodide has been synthesized and structurally determined. The $[PbI_4(I_3)_2]^{4-}$ mononuclear cluster of **1** is a seldom example with I_3^- coordinated to the lead center. Strong hydrogen bonds between $[PbI_4(I_3)_2]^{4-}$ clusters and $(PBPY\text{-}H)_2^{4+}$ dimmers lead to the generation of a 2-D layer. Its absorption spectrum was investigated, and lower energy band gap of 1.42 eV was explained by DFT calculation. Interestingly, **1** exhibits photocatalytic activity for the degradation of rhodamine B with the degradation ratio of 82.4%.

REFERENCES

(1) Wang, G. E.; Xu, G.; Liu, B. W.; Wang, M. S.; Yao, M. S.; Guo, G. C. Semiconductive nanotube array constructed from giant $[Pb^{II}_{18}I_{54}(I_2)_9]$ wheel clusters. *Angew. Chem. Int. Ed.* **2016**, 55, 514–518.

(2) Dammak, H.; Yangui, A.; Triki, S.; Abid, Y.; Feki, H. Structural characterization, vibrational, optical properties and DFT investigation of a new luminescent organic-inorganic material: $(C_6H_{14}N)_3Bi_2I_9$. *J. Lumin.* **2015**, 161, 214–220.

(3) Adonin, S. A.; Rakhmanova, M. E.; Smolentsev, A. I.; Korolkov, I. V.; Sokolov, M. N.; Fedin, V. P. Binuclear Bi(III) halide complexes with 4,4′-ethylenepyridinium cations: luminescence tuning by reversible salvation. *New J. Chem.* **2015**, 5529–5533.

(4) Xu, G.; Guo, G. C.; Guo, J. S.; Guo, S. P.; Jiang, X. M.; Yang, C.; Wang, M. S.; Zhang, Z. J. Photochromic inorganic-organic hybrid: a new approach for switchable photoluminescence in the solid state and partial photochromic phenomenon. *Dalton Trans*. **2010**, 39, 8688–8692.

(5) Xu, G.; Guo, G. C.; Wang, M. S.; Zhang, Z. J.; Chen, W. T.; Huang, J. S. Photochromism of a methyl viologen bismuth(III) chloride: structural variation before and after UV irradiation. *Angew. Chem. Int. Ed.* **2007**, 46, 3249–3251.

(6) Wang, M. S.; Xu, G.; Zhang, Z. J.; Guo, G. C. Inorganic-organic hybrid photochromic materials. *Chem. Commun.* **2010**, 46, 361–376.

(7) Gagor, A.; Weclawik, M.; Bondzior, B.; Jakubas, R. Periodic and incommensurately modulated phases in a (2-methylimidazolium)tetraiodobismuthate(III) thermochromic organic-inorganic hybrid. *CrystEngComm.* **2015**, 27, 3286–3296.

(8) Goforth, A. M.; Tershansy, M. A.; Smith, M. D.; Peterson Jr., L.; Kelley, J. G.; DeBenedetti, W. J.; zur Loye, H. C. Structural diversity and thermochromic properties of iodobismuthate materials containing *d*-metal coordination cations: observation of a high symmetry $[Bi_3I_{11}]^{2-}$ anion and of isolated I^- anions. *J. Am. Chem. Soc.* **2011**, 133, 603–612.

(9) Christians, J. A.; Fung, R. C. M.; Kamat, P. V. An inorganic hole conductor for organo-lead halide perovskite solar cells improved hole conductivity with copper iodide. *J. Am. Chem. Soc.* **2014**, 136, 758–764.

(10) Mosconi, E.; Amat, A.; Nazeeruddin, M. K.; Grätzel, M.; De Angelis, F. First-principles modeling of mixed halide organometal perovskites for photovoltaic applications. *J. Phys. Chem. C* **2013**, 117, 13902–13913.

(11) Zhang, Z. J.; Guo, G. C.; Xu, G.; Fu, M. L.; Zou, J. P.; Huang, J. S. $[(H_2en)_7(C_2O_4)_2]_n(Pb_4I_{18})_n$ $4nH_2O$, a new type of perovskite co-templated by both organic cations and anions. *Inorg. Chem.* **2006**, 45, 10028–10030.

(12) Aragoni, M. C.; Arca, M.; Caltagirone, C.; Devillanova, F. A.; Demartin, F.; Garau, A.; Isaia, F.; Lippolis, V. Inorganic-organic hybrid materials:

construction of the first polymeric channelled halometallate(II) system. *CrystEngComm.* **2005**, 7, 544–547.

(13) Wu, L. M.; Wu, X. T.; Chen, L. Structural overview and structure-property relationships of iodoplumbate and iodobismuthate. *Coord. Chem. Rev.* **2009**, 253, 2787–2804.

(14) Wakamiya, A.; Endo, M.; Sasamori, T.; Tokitoh, N.; Ogomi, Y.; Murata, Y. Reproducible fabrication of efficient perovskite-based solar cells: X-ray crystallographic studies on the formation of $CH_3NH_3PbI_3$ layers. *Chem. Lett.* **2014**, 43, 711–713.

(15) Louvain, N.; Mercier, N.; Luc, J.; Sahraoui, B. Example of disulfide conformational change in the solid state: preparation, optical properties, and X-ray studies of a cystamine-based iodoplombate hybrid. *Eur. J. Inorg. Chem.* **2008**, 3592–3596.

(16) Lin, R. G.; Xu, G.; Wang, M. S.; Lu, G.; Li, P. X.; Guo, G. C. Improved photochromic properties on viologen-based inorganic-organic hybrids by using π^-conjugated substituents as electron donors and stabilizers. *Inorg. Chem.* **2013**, 52, 1199–1205.

(17) Phillips, A. D.; Fei, Z.; Ang, W. H.; Scopelliti, R.; Dyson, P. J. A crystallographic story of snakes and ladders: encapsulated water polymers and rigid metal complexes based on mono-N-substituted carboxylate 4,4′-bipyridine. *Cryst.Growth Des.* **2009**, 9, 1966–1978.

(18) Perew, J. P.; Burke, K.; Ernzerhof, M. Generalized gradient approximation made simple. *Phy. Rev. Lett*. **1996**, 77, 3865–3868.

(19) Segall, M.; Probert, M.; Pickard, C.; Hasnip, P.; Clark, S.; Refson, K.; Payne, M. *Materials Studio CASTEP version 4.1* **2006**.

(20) Sheldrick, G. M. *SHELXS97 and SHELXL97*. University of Göttingen, Germany **1997**.

(21) Brown, D. J. Bond valence as an aid to understanding the stereochemistry of O and F complexes of Sn(II), Sb(III), Te(IV), I(V) and Xe(VI). *J. Solid. State. Chem.* **1974**, 11, 214–233.

(22) Svensson, P. H.; Kloo, L. Metal iodides in polyiodide networks: synthesis and structure of binary metal iodide-iodine compounds stable under ambient conditions. *Inorg. Chem.***1999**, 38, 3390–3393.

(23) Zhao, S. B.; Wang, R. Y.; Wang, S. N. Dinuclear Cu(I) complexes of 1,2,4,5-tetra(7-azaindolyl)benzene: persistent 3-coordinate geometry, luminescence, and reactivity. *Inorg. Chem.* **2006**, 45, 5830–5840.

(24) Wang, G. E.; Xu, G.; Liu, B. W.; Wang, M. S.; Yao, M. S.; Guo, G. C. Semiconductive nanotube array constructed from giant $[Pb_{18}I_{54}(I_2)_9]$ wheel clusters. *Angew. Chem. Int. Ed.* **2016**, 55, 514–518.

(25) Tong, Z.; Pu, S.; Xiao, Q.; Liu, G.; Cui, S. Synthesis and photochromism of a novel water-soluble diarylethene with glucosyltriazolyl groups. *Tetra. Lett.* **2013**, 54, 474–477.

(26) Sourisseau, S.; Louvain, N.; Bi, W.; Mercier, N.; Rondeau, D.; Boucher, F.; Buzare, J. Y.; Legein, C. Reduced band gap hybrid perovskites resulting from combined hydrogen and halogen bonding at the organic-inorganic interface. *Chem. Mater.* **2007**, 19, 600–607.

(27) Zhu, X. H.; Mercier, N.; Frere, P.; Blanchard, P.; Roncali, J.; Allain, M.; Pasquier, C.; Riou, A. Effect of mono- versus di-ammonium cation of 2,2′-bithiophene derivatives on the structure of organic-inorganic hybrid materials based on iodo metallates. *Inorg. Chem.* **2003**, 42, 5330–5339.

(28) Wendlandt, W. W.; Hecht, H. G. *Reflectance Spectroscopy*. Interscience Publishers: New York **1966**.

(29) Kotiim, G. *Reflectance Spectroscopy*. Springer-Verlag: New York **1969**.

(30) Baibarac, M.; Preda, N.; Mihut, L.; Baltog, I.; Lefrant, S.; Mevellec, J. Y. On the optical properties of micro- and nanometric size PbI_2 particles. *J. Phys. Condens. Matter.* **2004**, 16, 2345–2356.

(31) Yang, J.; Dolg, M. First-principles electronic structure study of the monoclinic crystal bismuth triborate BiB_3O_6. *J. Phys. Chem. B* **2006**, 110, 19254–19263.

(32) Horikoshi, S.; Saitou, A.; Hidaka, H.; Serpone, N. Environmental remediation by an integrated microwave/UV illumination method. V. Thermal and nonthermal effects of microwave radiation on the photocatalyst and on the photodegradation of rhodamine-B under UV/Vis radiation. *Environ. Sci. Technol.* **2003**, 37, 5813–5822.

Table 1. Selected Bond Lengths (Å) and Bond Angles (°)

Bond	Dist.	Bond	Dist.	Bond	Dist.
Pb(1)–I(1)#1	3.124(6)	Pb(1)–I(1)	3.124(6)	Pb(1)–I(2)#1	3.173(2)
Pb(1)–I(2)	3.173(2)	Pb(1)–I(3)#1	3.317(7)	Pb(1)–I(3)	3.317(7)
I(3)–I(4)	2.961(8)	I(4)–I(5)	2.881(1)		
Angle	(°)	Angle	(°)	Angle	(°)
I(5)–I(4)–I(3)	176.4(3)	I(1)#1–Pb(1)–I(2)#1	90.1(6)	I(1)–Pb(1)–I(2)#1	89.8(3)
I(1)#1–Pb(1)–I(2)	89.8(3)	I(1)–Pb(1)–I(2)	90.1(6)	I(3)#1–Pb(1)–I(3)	180.0(0)

Symmetry code: #1 $-x+1, -y, -z$

Table 2. Hydrogen Bond Details in 1

D–H ···A	d(D–H)	d(H ···A)	∠DHA	d(D ···A)	Symmetry code
O(2)–H(2C) ··O(1)	0.82	1.87	161	2.662(8)	2–*x*, 2–*y*, 1–*z*
N(2)–H(2) ··I(2)	0.73(7)	2.89(8)	153(8)	3.557(7)	
C(12)–H(12) ··I(1)	0.93	3.03	140	3.788(8)	*x*, 1/2–*y*, 1/2+*z*

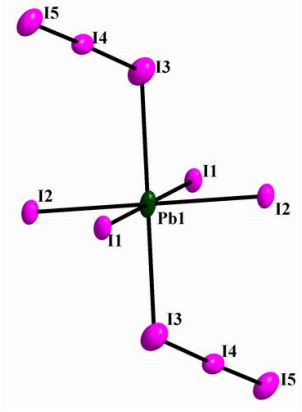

(a)

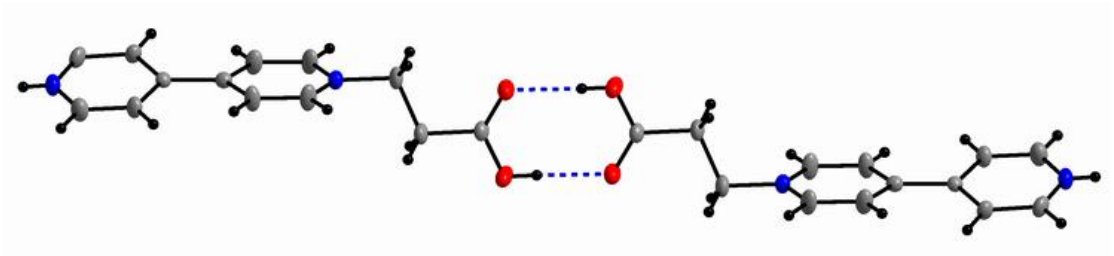

(b)

Fig. 1. (a) Structure of $[PbI_4(I_3)_2]^{4-}$ mononuclear cluster; (b) $(PBPY\text{-}H)_2^{4+}$ dimmer constructed from hydrogen bonds

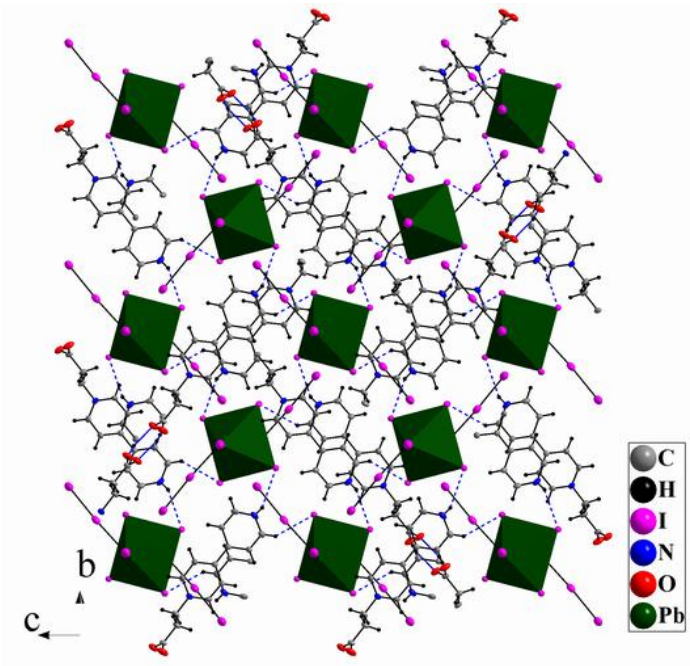

Fig. 2. $(PBPY\text{-}H_2)_2[PbI_4(I_3)_2]$ 2-D layer based on O-H ··O, N-H ··I and C-H ··I hydrogen bonds

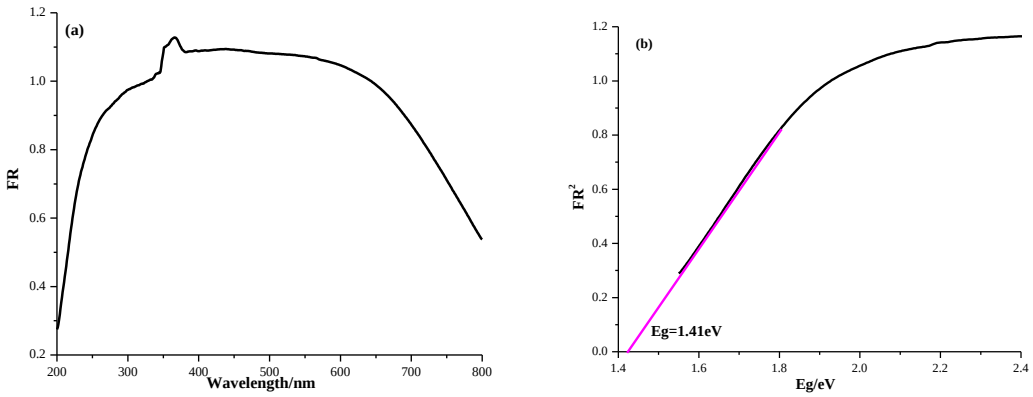

Fig. 3. Room temperature UV-Vis absorption spectrum (a) and diffuse reflectance spectrum in Kubelka-Munk unit (b) of 1

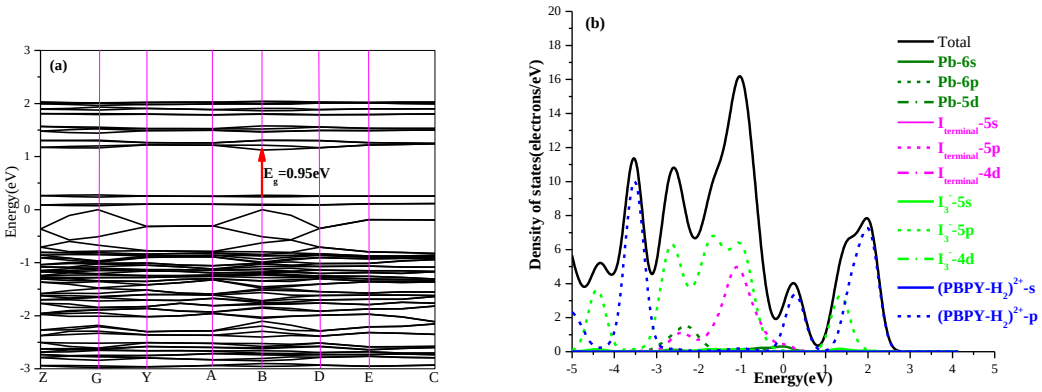

Fig. 4. (a) Band structure and (b) density of states based on DFT calculaiton

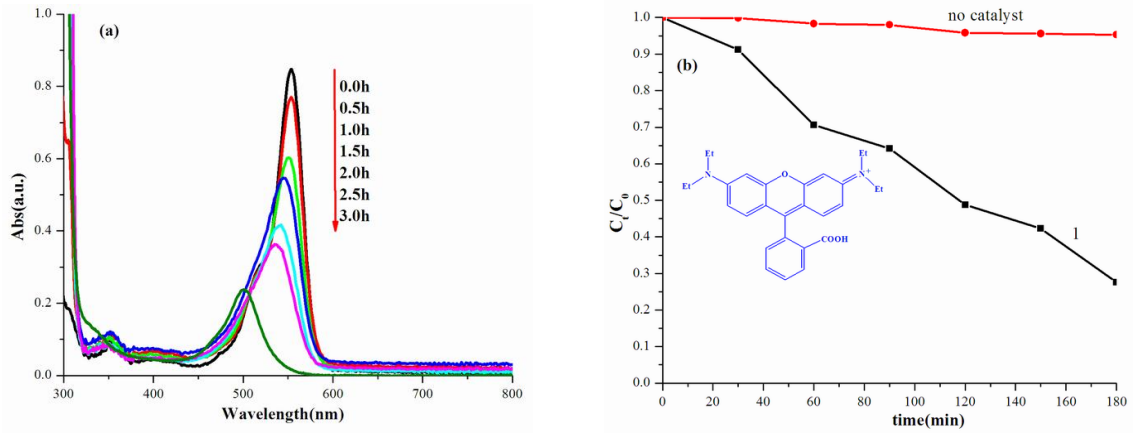

Fig. 5. (a) Time-dependent UV-Vis spectra of RhB in the presence of 1 under the irradiation of xenon-lamp; (b) Concentration change of RhB. C_t and C_0 stand respectively for the RhB concentrations after and before irradiation

A New Iodiplumbate-based Hybird Constructed from Asymmetric Viologen and Polyiodides: Structure, Properties and Photocatalytic Activity for the Degradation of Organic Dye

WANG Dao-Hua(王道华)　LIN Xiao-Yan(林小燕)　WANG Yu-Kang(王雨康)

ZHANG Wen-Ting(张文婷)　SONG Kai-Yue(宋凯悦)　LIN Heng(林恒)

LI Hao-Hong(李浩宏)　CHEN Zhi-Rong(陈之荣)

A new iodiplumbate/organic hybrid constructed from asymmetric viologen and polyiodides has been synthesized, which is a seldom example with I_3^- coordinated to the lead center. The lower energy band gap of 1.42 eV was explained by DFT calculation, and compound **1** exhibits photocatalytic activity for the degradation of rhodamine B with the degradation ratio of 82.4%.